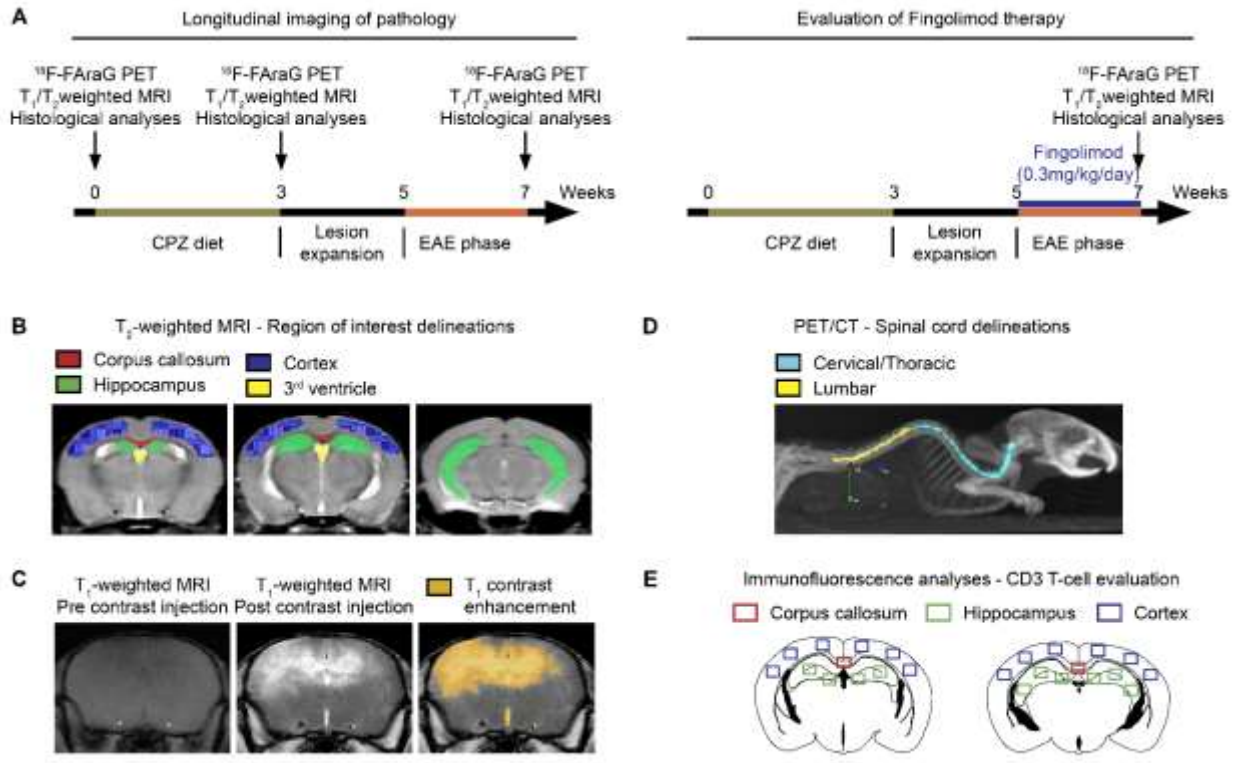

Supplemental Figure 1.

(A) Experimental outline indicates the timeline of the CPZ-EAE model induction, Fingolimod treatment, *in vivo* PET/ CT and MRI time points, and histological analyses. (B) Representative example of regions of interests (ROIs) delineated on T_2-weighted images for the corpus callosum (red), hippocampus (green), cortex (dark blue) and 3rd ventricle (yellow). (C) Representative T_1-weighted MR image obtained prior and after injection of gadolinium, and corresponding delineation of T_1 signal contrast enhancement (orange). (D) Representative CT image showing the delineation of the cervical/ thoracic (light blue) and lumbar (yellow) spinal cord segments. (E) Schematic illustration of brain regions used for evaluation of CD3 T-cell number in the corpus callosum (red, 2 regions), hippocampus (green, 8-10 regions) and cortex (dark blue, 10-12 regions).

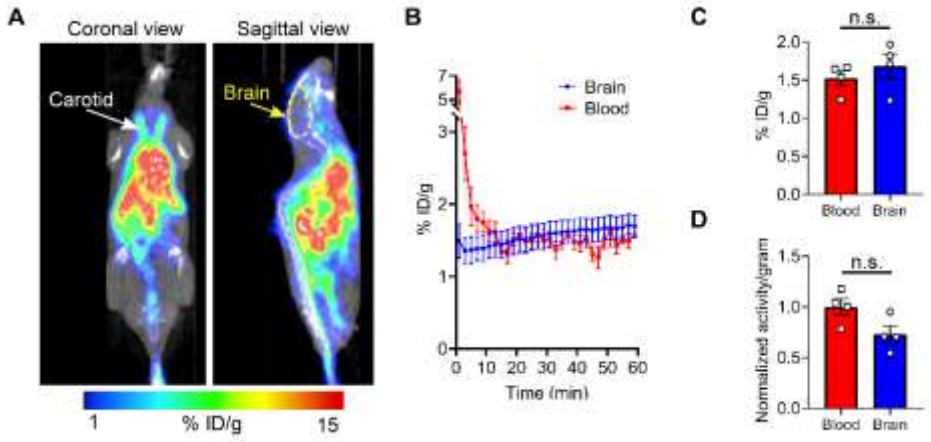

Supplemental Figure 2.

(A) Representative ^{18}F-FAraG PET/ CT image of a control mouse acquired during the first 2 minutes following iv injection of ^{18}F-FAraG. ^{18}F-FAraG signal can be detected in the left and right carotids (white arrow). The brain area used to measure ^{18}F-FAraG signal from the brain tissue is indicated by a dashed yellow line. (B) Time-activity curves from the blood and brain indicating steady accumulation of ^{18}F-FAraG into the brain tissue. (C) No significant differences were observed between ^{18}F-FAraG levels in the blood and brain, calculated from the averaged mean of the last 10 minutes of dynamic PET acquisition. Brain-to-blood ratio calculated from PET images is 1.1±0.2. (D) No significant differences were observed between the normalized blood and brain^{18}F-FAraG levels quantified from *ex vivo* biodistribution studies. Brain-to-blood ratio calculated from *ex vivo* biodistribution studies is 0.73±0.1. n.s. not significant.

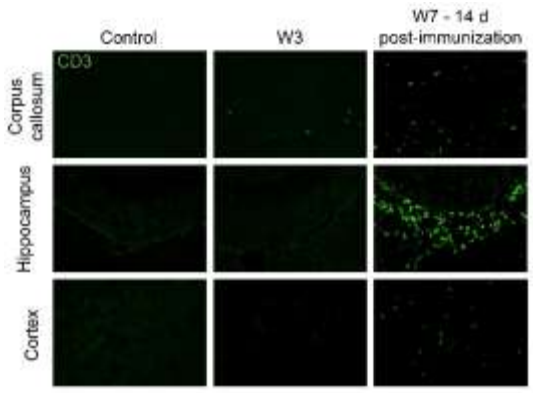

Supplemental Figure 3.

Representative immunofluorescence images showing low CD3 T-cells infiltration in the corpus callosum at W3, and elevated CD3 T-cells infiltration in the corpus callosum, hippocampus and cortex at W7.

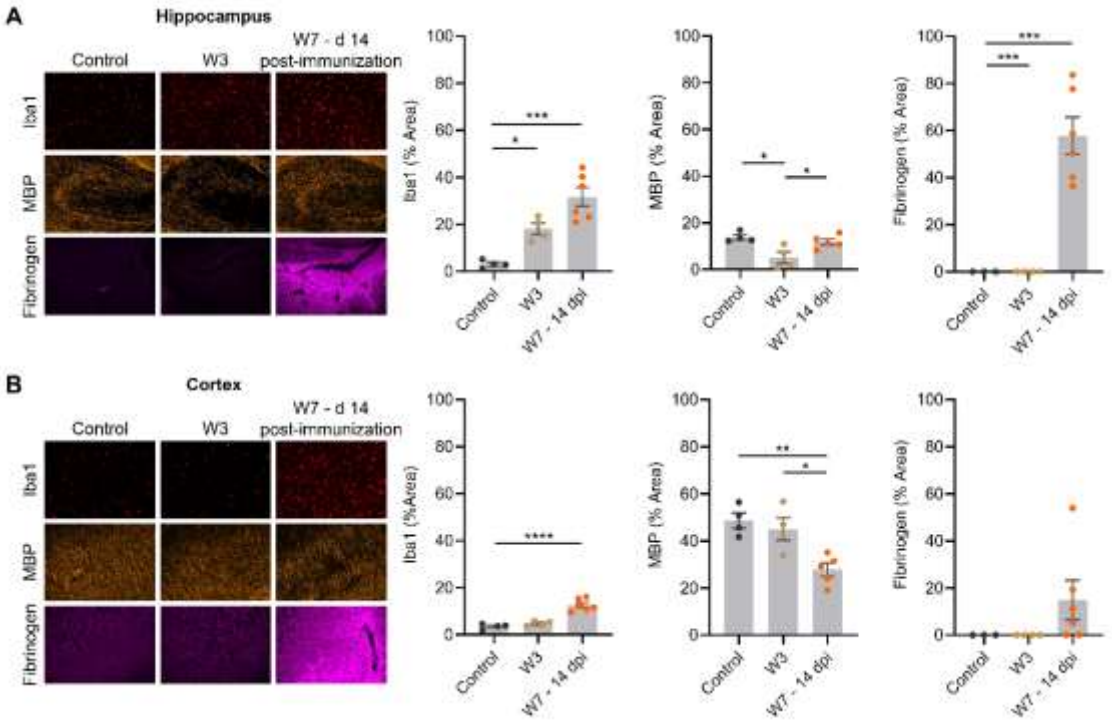

Supplemental Figure 4.

(A) Representative immunofluorescence images from the hippocampus in control animals, at W3 and W7 for microglia/ macrophages (Iba1, red), myelin basic protein (MBP, orange) and fibrinogen (pink). Quantitative analyses indicated a significant increase of microglia/ macrophages (Iba1) at W3 and W7. Demyelination was observed through a decrease of MBP at W3 only. Note that spontaneous remyelination occurred between W3 and W7. Important fibrinogen deposition was detected at W7 for all individuals. (B) Representative immunofluorescence images from the cortex in controls, at W3 and W7 for microglia/ macrophages (Iba1, red), myelin basic protein (MBP, orange) and fibrinogen (pink). Quantitative analyses indicated a significant increase of microglia/ macrophages (Iba1) at W7. Patchy cortical demyelination was observed at W7, and fibrinogen deposition was detected at W7 only in a subset of animals *(*p≤0.05, **p≤0.01, ***p≤0.001, ****p≤0.0001*).

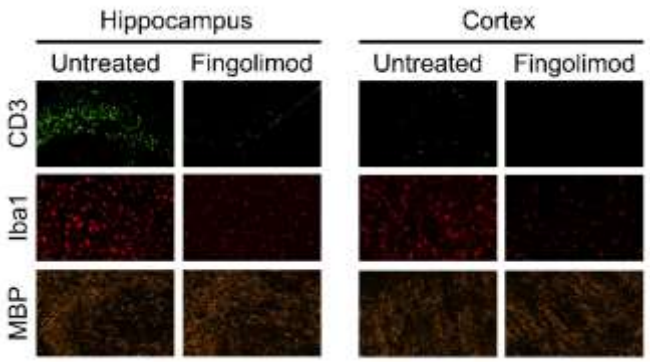

Supplementary Figure 5.

Representative immunofluorescence analyses of the hippocampus and cortex for untreated and Fingolimod-treated animals at W7 for CD3 T-cells (green), microglia/ macrophages (Iba1, red), and myelin basic protein (MBP, orange) showing lower number of CD3 T-cells and microglia/ macrophages in Fingolimod-treated compared to untreated mice, and no difference in myelin.

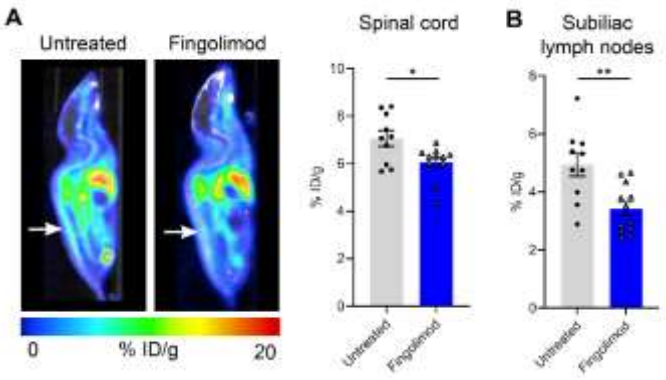

Supplemental Figure 6.

(A) Representative ^{18}F-FAraG PET/ CT images and quantitative analyses indicate lower ^{18}F-FAraG signal in the spinal cord (arrows) of Fingolimod-treated mice compared to untreated mice. (B) Similarly, quantitative analyses revealed significantly lower ^{18}F-FAraG signal in the subiliac lymph nodes of Fingolimod-treated mice compared to untreated mice *(*$p \leq 0.05$, **$p \leq 0.01$)*.

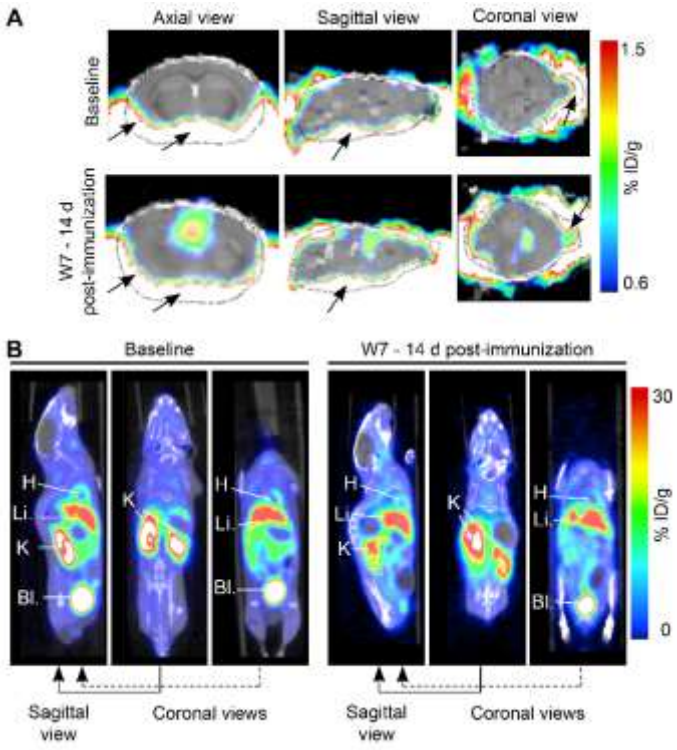

Supplemental Figure 7.

(A) ^{18}F-FAraG PET/ CT images overlaid on T_2w MR images showing different sections of the brain from a representative mouse at Baseline and W7-14dpi. ^{18}F-FAraG images indicate higher signal uptake in regions closer to the ventral part of the brain at Baseline and W7+14dpi (black arrows). (B) ^{18}F-FAraG PET/ CT images of the entire mouse body from a representative mouse at Baseline and at W7-14dpi showing accumulation of ^{18}F-FAraG in peripheral organs including liver (Li.), heart (H), kidneys (K) and bladder (Bl.).

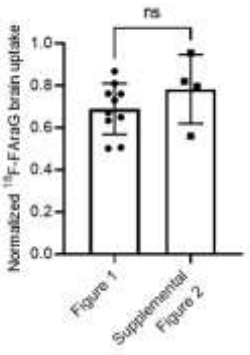

Supplemental Figure 8.

^{18}F-FAraG signal in the brain normalized to ^{18}F-FAraG signal in the leg muscles, shown for the two cohort of control mice (Figure 1 and Supplemental Figure 2). No statistical difference was found between the normalized ^{18}F-FAraG signal in the brain between these two cohorts of control mice (*p=0.2575*).

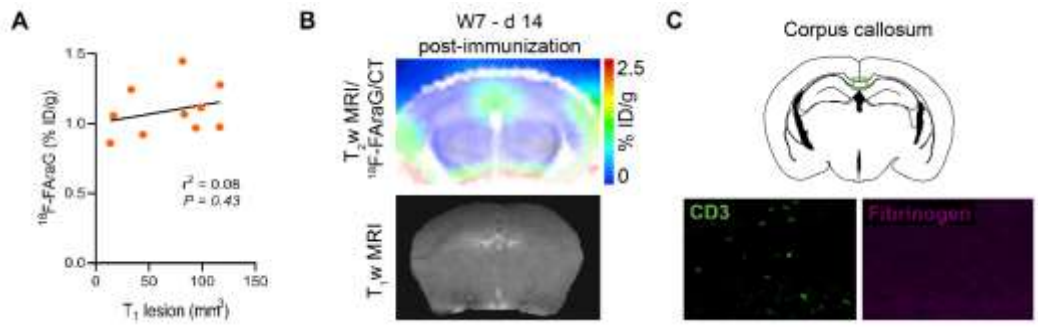

Supplemental Figure 9.

(A) ^{18}F-FAraG signal did not correlate to the T_1 enhancing lesion volume (r^2 = 0.08, *p = 0.43*). (B) Representative ^{18}F-FAraG PET/ CT overlaid on T_2w MRI and corresponding T_1w MRI indicating increased ^{18}F-FAraG signal in the corpus callosum but no T_1 enhancing lesion. (C) Corresponding immunofluorescence images confirmed the presence of CD3 T-cells in the corpus callosum and no BBB alteration indicated by no fibrinogen deposition.